JCB Article

Cation–chromatin binding as shown by ion microscopy is essential for the structural integrity of chromosomes

Reiner Strick,[1] Pamela L. Strissel,[1] Konstantin Gavrilov,[2] and Riccardo Levi-Setti[2]

[1]Division of Biological Sciences, Department of Medicine, and [2]Division of Physical Sciences, Enrico Fermi Institute and Department of Physics, University of Chicago, Chicago, IL 60637

Mammalian interphase and mitotic cells were analyzed for their cation composition using a three-dimensional high resolution scanning ion microprobe. This instrument maps the distribution of bound and unbound cations by secondary ion mass spectrometry (SIMS). SIMS analysis of cryofractured interphase and mitotic cells revealed a cell cycle dynamics of Ca^{2+}, Mg^{2+}, Na^{+}, and K^{+}. Direct analytical images showed that all four, but no other cations, were detected on mitotic chromosomes. SIMS measurements of the total cation content for diploid chromosomes imply that one Ca^{2+} binds to every 12.5–20 nucleotides and one Mg^{2+} to every 20–30 nucleotides. Only Ca^{2+} was enriched at the chromosomal DNA axis and colocalized with topoisomerase IIα (Topo II) and scaffold protein II (ScII). Cells depleted of Ca^{2+} and Mg^{2+} showed partially decondensed chromosomes and a loss of Topo II and ScII, but not hCAP-C and histones. The Ca^{2+}-induced inhibition of Topo II catalytic activity and direct binding of Ca^{2+} to Topo II by a fluorescent filter-binding assay supports a regulatory role of Ca^{2+} during mitosis in promoting solely the structural function of Topo II. Our study directly implicates Ca^{2+}, Mg^{2+}, Na^{+}, and K^{+} in higher order chromosome structure through electrostatic neutralization and a functional interaction with nonhistone proteins.

Introduction

Although multiple indirect experiments have proven the over 70-yr-old hypothesis that DNA in nuclei is complexed with monovalent and divalent cations (Hammarsten, 1923), there have only been a few attempts to obtain direct three-dimensional (3D)* high resolution images of cations in cells and on chromosomes without the use of secondary fluorescent indicators (Kearns and Sigee, 1980; Chandra et al. 1984; Horoyan et al., 1992). To date, all cellular cation distributions have only been shown at a spatial resolution ≥500 nm and, in addition, even less is known regarding specific interactions between cations and chromatin-binding proteins and their influence on chromosome structure. Therefore, revealing cation distributions and cation–protein interactions in cells is important to understand the roles of cations during the cell cycle and in the maintenance of higher order chromosome structure.

The most abundant cations in the eukaryotic cell are Ca^{2+}, Mg^{2+}, Na^{+}, and K^{+}. These cations are fundamental for multiple cellular processes in every phase of life including cell growth and differentiation, development, cell–cell interactions, morphology, motility, and apoptosis leading to cell death (for review see Boynton et al., 1982). The major Ca^{2+} storage sites in the cell are the ER, Golgi complex, mitochondria, secretory granules, and nuclear envelope (for review see Rottingen and Iversen, 2000). The K^{+} storage sites are mainly the cytosol, Golgi complex, and the nucleus (Schapiro and Grinstein, 2000). Multiple ion transmembrane pumps (ATPases) and exchangers are responsible for Ca^{2+}, Mg^{2+}, Na^{+}, and K^{+} cellular influx and efflux to regulate the cellular cation concentrations from internal storage sites and to maintain osmolarity (for review see Scheiner-Bobis, 1998).

Cations have been implicated in the regulation of the cell cycle (for reviews see Boynton et al., 1982; Hepler, 1994). For example, increasing concentrations of Ca^{2+}, Mg^{2+}, and

Address correspondence to Reiner Strick, Dept. of Medicine, University of Chicago, 5841 S. Maryland Ave., MC2115, Chicago, IL 60637-1470. Tel.: (773) 834-1539. Fax: (773) 702-3002.

E-mail: rstrick@medicine.bsd.uchicago.edu

R. Strick and P. Strissel contributed equally to this work.

*Abbreviations used in this paper: 3D, three-dimensional; AT, adenine-thymine; BAPTA, 1,2-bis[o-aminophenoxy]ethane-*N*,*N*,*N*′,*N*′-tetraacetic acid; IM, Indian muntjac; ISI, ion-induced secondary ion; PVDF, polyvinyldifluoride; SAR, scaffold-associated region; ScII, scaffold protein II; SIMS, secondary ion mass spectrometry; Topo II, topoisomerase IIα.

Key words: cations; chromosome structure; condensation; ion microscopy; topoisomerase II

Na^+ in the media of growing cells stimulated the mitotic rate almost twofold, whereas in contrast, K^+ had no effect (Atkinson et al., 1983). In other studies, cellular Na^+ concentration levels appeared to fluctuate throughout the cell cycle peaking in M and S phase, whereas the K^+ nuclear and cytoplasmatic concentration levels remained unchanged (Cameron et al., 1979; Warley et al., 1983). Several studies have implicated a major role of Ca^{2+} in mitosis, correlating with nuclear envelope breakdown and entry into mitosis, microtubular breakdown at the meta- to anaphase transition, and a brief Ca^{2+} increase at the anaphase onset (Poenie et al., 1986), which led to activated chromosome motion (Groigno and Whitaker, 1998). The meta- to anaphase transition could be prevented with EGTA or the more specific Ca^{2+}-chelator 1,2-bis[o-aminophenoxy]ethane-*N*,*N*,*N*′,*N*′-tetraacetic acid (BAPTA) in Ca^{2+}-free medium (for review see Hepler, 1994).

The main cations interacting with DNA are Ca^{2+}, Mg^2, Na^+, and K^+. The divalent cations bind to the negatively charged phosphate residues of DNA in a stoichiometry of 1 mol Ca^{2+} or Mg^{2+} to 2 mol phosphate (e.g., Mathieson and Olayemi, 1975). Recent crystallization studies of B-DNA decamers or dodecamers in the presence of Mg^{2+} or Ca^{2+} confirmed a direct cation interaction with the major and minor grooves as well as phosphate oxygen atoms contributing to DNA stabilization and conformation (Minasov et al., 1999; Chiu and Dickerson, 2000). These crystallization studies resolved that Ca^{2+} has a higher affinity to DNA, inducing a greater DNA bending and thermal stabilization than Mg^{2+}.

Several studies have shown that mono- and divalent cations are essential in maintaining higher order chromatin structure. For example, chromatin at low ionic strength and in the absence of divalent cations has an extended structure representing the 10-nm coil. The transformation to a more compact or 30-nm structure, that is described as a solenoid or arrangement of superbeads, could be induced by an increase of Na^+ or Mg^{2+} and Ca^{2+} (for review see Felsenfeld and McGhee, 1986). Models of mitotic chromosome structures have been proposed for the folding of the chromatin fiber >30 nm, each based on the hierarchical organization of eukaryotic chromatin into loops and coils (Ohnuki, 1968; Rattner and Lin, 1985; Filipski et al., 1990). In the loop-scaffold model, highly ademine-thymine (AT)-rich DNA elements, named scaffold-associated regions (SARs) interact dynamically with nonhistone proteins to form loop anchorage sites (Paulson and Laemmli, 1977). SARs play a key role as cis elements of chromosome dynamics and as initiation elements for chromosome condensation (Strick and Laemmli, 1995). Nonhistone binding proteins like topoisomerase IIα (Topo II) and scaffold protein II (ScII) (homologue to hCAP-E, an SMC protein), have been implicated as partners in a nuclear complex (Ma et al., 1993) and also colocalize at the chromosomal axis (Lewis and Laemmli, 1982; Saitoh et al., 1994). Topo II and protein complexes, called condensins, including hCAP-C and -E and other SMC proteins, are essential for chromosome condensation, structure maintenance, and sister chromatid separation (Adachi et al., 1991; Schmiesing et al., 1998; Hirano, 1999).

There are several methodologies available to measure both free and bound cations in cells. Fluorescent indicators, like fura-2 were developed to detect free cations, especially Ca^{2+} (Poenie et al., 1986). However, these indicators encounter several technical problems; for example, they can bind nonspecifically to cell constituents or other cations (McCormack and Cobbold, 1991). Although X-ray crystallography can detect Ca^{2+} and Mg^{2+} on DNA oligonucleotides (Minasov et al., 1999), Na^+ and K^+ cannot be easily distinguished because of the interference with H_2O. In addition, cryogenic temperatures and crystal packing effects occurring during X-ray crystallography may shift the ion distribution of the sample. X-ray microanalysis has been used to measure cations in the nucleus and cytoplasm during the cell cycle (Cameron et al., 1979; Warley et al., 1983). Although this technique involves lengthy exposures and needs substantial spectral corrections due to the presence of a high continuous background, this method is a valuable tool for chemical quantitation.

In contrast to X-ray microanalysis, which determines the atomic composition only at specific points within a biological sample and with no direct microscopic representation and depth information, secondary ion mass spectrometry (SIMS) (Benninghoven, 1987) measures the isotopic composition either in the form of stable or tracer isotopes with high sensitivity, high spatial resolution, and essentially no background. Previous SIMS investigations using BrdU-labeled human and polytene chromosomes demonstrated the use of tracer isotopes (Levi-Setti et al., 1997). SIMS signals provide a rapid visualization of the isotopic distribution within a sample, and SIMS sequential mapping renders in-depth analytical information for constructing 3D compositional images (SIMS tomography).

In this investigation, we show for the first time high-resolution analytical images of the cation composition of mammalian interphase and mitotic cells as well as of isolated metaphase chromosomes using the University of Chicago (Chicago, IL) scanning ion microprobe (Levi-Setti, 1988; Chabala et al. 1995). To preserve the ionic integrity of the analyzed cells and prevent the well-known occurrence of analytical artifacts due to the high diffusivity of cations in biological samples (Morgan et al., 1975), we used fast cryopreservation methods (freeze drying and freeze fracture) (Echlin, 1984), without any prefixations or washes. This study presents SIMS imaging evidence of cation redistribution between cytosol and chromosomes during the cell cycle and proves that Mg^{2+}, Ca^{2+}, K^+, and Na^+ are an integral part of mitotic chromatin. Our results indicate that Ca^{2+} directly binds to Topo II in the absence of DNA, supporting a regulatory role of Ca^{2+} in the reversible transition of a catalytically active Topo II to a structural DNA binding protein during mitosis.

Results

Cryopreserved and fractured interphase and mitotic cells show cell cycle dynamics of cations

3D-SIMS analysis of cryopreserved and cryofractured Indian muntjac (IM) deer fibroblasts showed a specific cation distribution inside the cell and throughout the cell cycle (Fig. 1, A–E). In interphase cells $^{40}Ca^{2+}$ distributed throughout the cytosol with specific accumulations, possi-

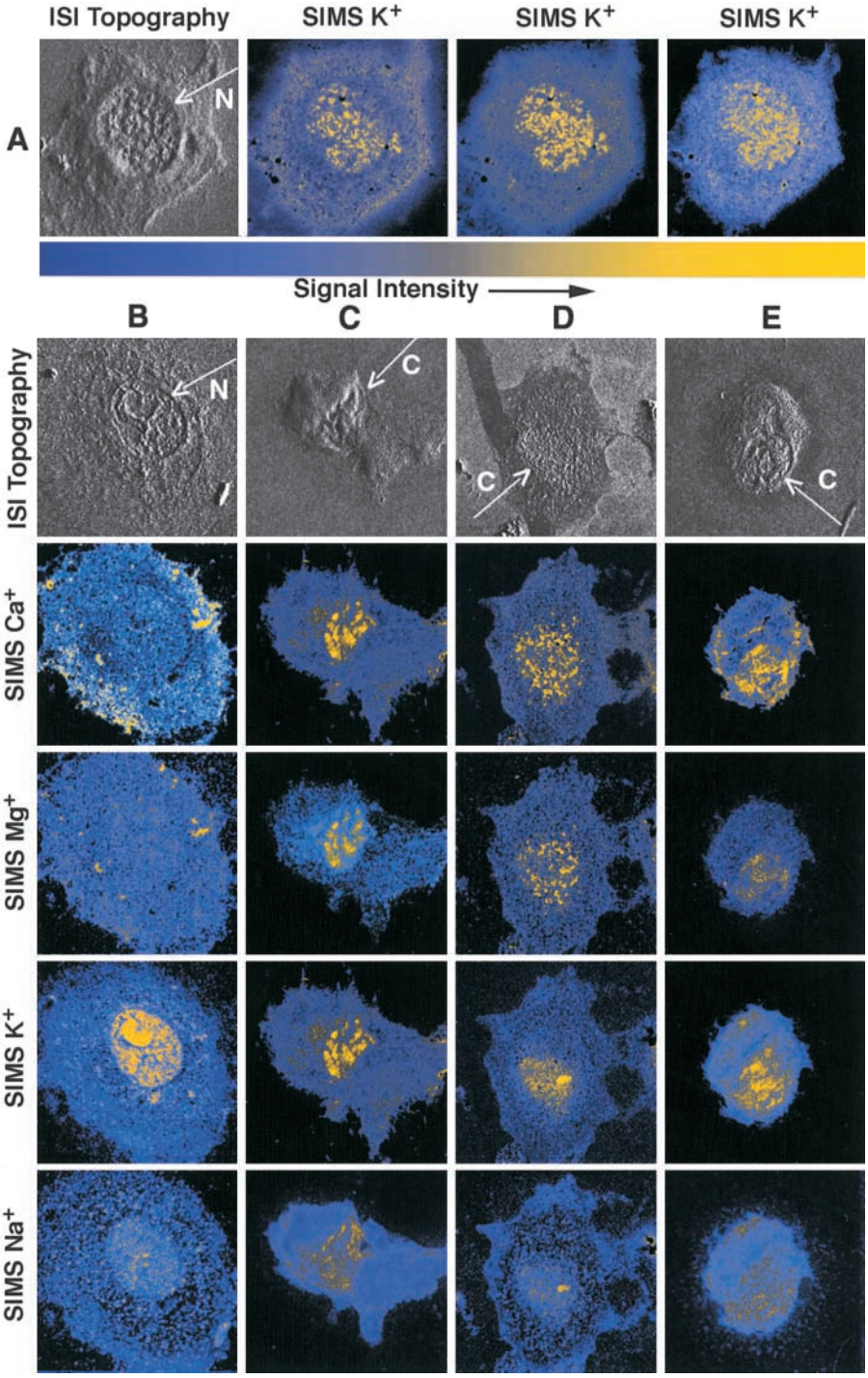

Figure 1. **(A) SIM images of an IM fibroblast interphase cell.** The total ISI image represents the cell topography. The three SIMS $^{39}K^+$ distributions in the cell are obtained at increasing erosion depths in steps of ~20 nm (left to right). The color strip below represents the pseudocolor scale associated with the SIMS intensities. (B–E) ISI and SIMS distributions for $^{40}Ca^{2+}$, $^{24}Mg^{2+}$, $^{39}K^+$, and $^{23}Na^+$ for interphase (B) and mitotic IM cells (C–E). Note that the uneven fracturing of the mitotic cell (E) could be responsible for the halfring-like structure around the chromatin. Each panel represents one example IM cell analyzed for the different cations. N, nucleus; C, chromosomes. Fields of view: (A, B, and C) 44 μm; (D) 66 μm; (E) 55 μm.

bly representing the ER and Golgi complex, whereas the nucleus was reduced of Ca^{2+} (Fig. 1 B). In contrast to interphase, mitotic cells showed high concentrations of Ca^{2+} on chromatin (Fig. 1, C–E). A similar distribution was detected for $^{24}Mg^{2+}$ in interphase and mitotic cells (Fig. 1, B–E). A SIMS analysis of 10 nocodazole-arrested IM cells demonstrated Ca^{2+} and Mg^{2+} enrichment on mitotic chromatin. A colocalization of these cations with mitotic chromatin could be proven using $^{81}Br^-$dU as a tracer for DNA (Fig. 2). In contrast to Ca^{2+} and Mg^{2+}, the monovalent cations $^{23}Na^+$ and $^{39}K^+$ remained unchanged in their cellular distribution throughout the cell cycle. Na^+ in interphase and mitotic cells distributed throughout the entire cytosol and nucleus and associated with mitotic chromatin. K^+ was enriched in the nucleus and especially in the nucleolus during interphase and also on chromatin during mitosis (Fig. 1, A–E). Fig. 1 A shows three successive K^+ layers of an entire interphase cell. The first layer shows in addition to the nucleus positive K^+ signals at the rim of the cell, which could represent Na^+/K^+ ATPase pumps and K^+ channels. Using SIMS, we observed that omitting buffer washes of cells before the cryopreservation maintained morphology and consistent cation distributions among multiple samples tested (unpublished data).

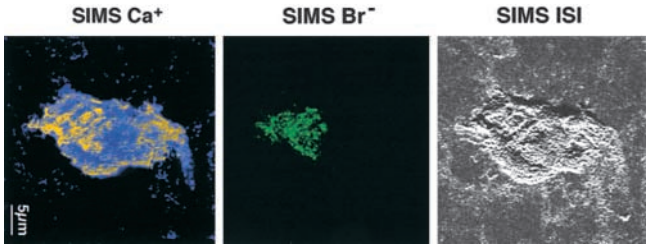

Figure 2. **ISI and SIMS distributions for $^{81}Br^-$ (green) and $^{40}Ca^{2+}$ (yellow) in an IM mitotic cell.** Note the colocalization of the DNA incorporated Br^- and chromatin associated Ca^{2+}. Refer to the legend to Fig. 1 for SIMS Ca^{2+} intensities.

Specific cations are a fundamental part of mammalian metaphase chromosomes

The specific association of $^{40}Ca^{2+}$, $^{24}Mg^{2+}$, $^{39}K^+$, and $^{23}Na^+$ with mitotic chromatin in cryopreserved cells led to a further analysis of fractionated metaphase chromosomes for cation binding using SIMS. To rule out methodological artifacts, we used two different chromosome harvesting and fixation procedures with IM and human BV173 cells. Both methods resulted in similar SIMS cation maps of chromosomes, where Ca^{2+}, Mg^{2+}, K^+, and Na^+ signals followed the chromatids (Fig. 3, A–D). However, we observed that fractionated *p*-formaldehyde–fixed chromosomes were more compact, rigid, and impervious to erosion with the ion probe than fractionated methanol-acid fixated chromosomes (Fig. 3 C). We also tested simultaneously the same chromosomal preparations for six additional specific divalent cations, like $^{55}Mn^{2+}$, $^{56}Fe^{2+}$, $^{58}Ni^{2+}$, $^{59}Co^{2+}$, $^{63}Cu^{2+}$, and $^{65}Zn^{2+}$. SIMS analysis demonstrated that these tested divalent cations were not associated with IM and BV173 chromosomes (unpublished data).

The specific binding of Ca^{2+} and Mg^{2+} was investigated further by SIMS to search for chromosome substructures, such as the chromosome axes, for example. To visualize the chromosome axes, which contain AT-rich DNA (Saitoh and Laemmli, 1994), IM cells were grown in the presence of the thymidine analogue BrdU (Levi-Setti et al., 1997). BrdU-labeled metaphase chromosomes at the second cell division (where the label content of sister chromatids is in the ratio 2:1) were then analyzed for $^{81}Br^-$, $^{40}Ca^{2+}$, and $^{24}Mg^{2+}$. As shown in Fig. 4, A and B, the $^{81}Br^-$ (as seen for the doubly Br^--labeled chromatid), and Ca^{2+} signals were both localized at the AT-rich axes, whereas Mg^{2+} was more equally distributed over the entire chromatid. The $^{26}CN^-$ map, (Fig. 4 C) representing the overall protein/DNA chromosomal profile, is broader than those of Br^- and Ca^{2+}. The Br^-/Ca^{2+} colocalization was further examined by obtaining average signal intensity profiles of Br^-, Ca^{2+}, and CN^- (counts/pixel), measured across the chromatids and plotted as a function of distance (μm) from the chromosomal symmetry axis (Fig. 4, D–F). We found that the Br^- signals peaked at ~0.3 μm (setting the chromosomal symmetry axis as 0 μm), and the maximal Ca^{2+} signals occurred at 0.3–0.5 μm, at the chromatid axis. In contrast, the CN^- map, signifying the chromatid borders (0–1.0 μm) showed a valley at the Ca^{2+} peak. At the chromosomal symmetry axis (0 μm), we detected a Ca^{2+} and Br^- valley, but a sharp

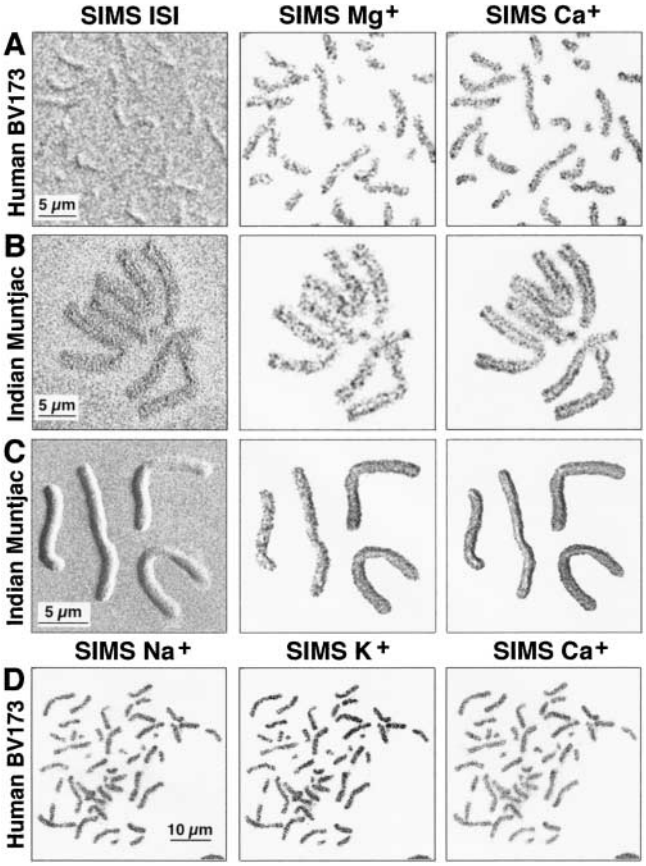

Figure 3. **Cation distribution on chromosomes using SIMS.** SIMS analytical distribution maps of $^{24}Mg^{2+}$ and $^{40}Ca^{2+}$ in chromosomes from BV173 (A and D) and IM chromosomes (B and C). Note that the cation signals follow along the chromatids for methanol-acetic acid fixed chromosomes (A and D), and for fractionated chromosomes fixed in methanol-acetic acid (B) or 4% *p*-formaldehyde (C).

CN^- peak, indicating a protein enriched region (Fig. 4 F). The structure of metaphase chromosomes is described in many different models, which also can coexist, like radial loops and helical coils (Rattner and Lin, 1985). This study shows a tripartite chromosomal structure, a center, axes, and an outer chromatid region, but does not reveal if loops or coils or both are present.

Interestingly, 10% of chromosomes showed a more refined coiling pattern for Ca^{2+} along the AT-rich axes, which appears to mimic the distribution of the main scaffold proteins Topo II and ScII (Fig. 5). We also observed that, in some of these cases, each Ca^{2+}/sister chromatid coiling was in opposite helicity, as described by Ohnuki (1968) and Boy de la Tour and Laemmli (1988) (unpublished data). Our results imply that Ca^{2+} colocalizes with Topo II and ScII at the chromatid axes.

Cation quantitation on chromosomes

The Ca^{2+} and Mg^{2+} cell and chromosome concentration measurements shown in Table I were obtained from the SIMS images by averaging the signal intensities over the entire cell, cellular compartments or chromosomes and using the calibration plots of Fig. 4, G and H. For example, we determined the total Ca^{2+} concentration of a cryopreserved in-

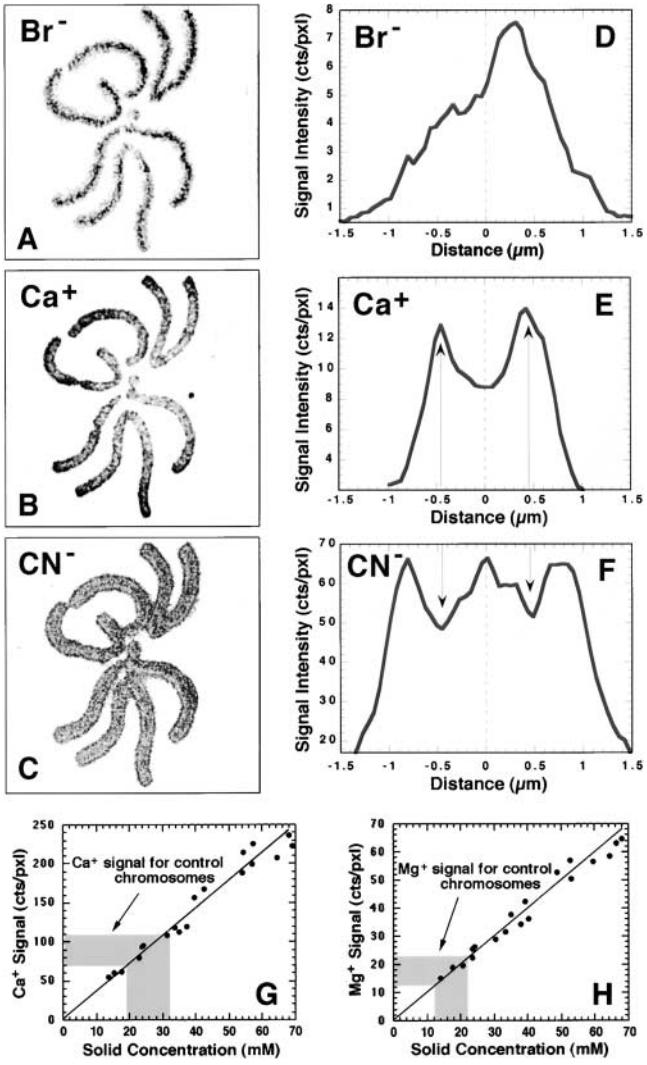

Figure 4. **Ca^{2+} colocalizes with AT-rich DNA on chromosomes.** (A,B, and C) SIMS analytical distribution maps of $^{81}Br^-$, $^{40}Ca^{2+}$, and $^{26}CN^-$ of BrdU-labeled IM metaphase chromosomes at the second cell division, where the sister chromatids label intensities are in the ratio 2:1 (shown in inverted contrast). The transverse signal intensity profiles (D,E, and F), averaged over the chromosomal length, were measured in counts per pixel (cts/pxl) and plotted versus the distance (in μm) from the chromosome symmetry axis (0 μm). The Br^- signal profile (D) peaks along the axis of the doubly labeled chromatid. The Ca^{2+} signal profile (E) (measured over the same set of segments chosen for the Br^- profile in D) peaks along both AT-rich axes, colocalizing with the Br^- peak. The CN^- SIMS map (C), which provides the overall protein and DNA profile, shows decreases in signal intensity (F) in contrast to the peaks of the Ca^{2+} and Br^- signals observed in D and E, respectively. Calibration plots of the SIMS signal intensity (cts/pxl) versus solid concentration (mM) of Ca^{2+} and Mg^{2+} are shown in G and H, respectively. The plotted points refer to concentration standards for these cations using agarose as a matrix. The shaded bands refer to the range of SIMS signal intensities and corresponding cation concentrations for the diploid karyotype.

terphase IM cell as 7.0–9.0 mM; and of a mitotic IM, cell 4.0–8.0 mM ($n = 6$). In contrast, the total Mg^{2+} concentration of an interphase and mitotic IM cell was 1.0–3.0 mM, respectively. In addition, we determined that the averaged divalent cation concentrations for a diploid set of chromosomes are for Ca^{2+} in the range of 20–32 mM; and for Mg^{2+}, 12–22 mM ($n = 15$) (Table I; Fig. 4, G and H). Assuming there are 6×10^9 DNA base pairs in a diploid eukaryotic cell, we calculated ratios of one Ca^{2+} for every 12.5–20 nucleotides and one Mg^{2+} for every 20–30 nucleotides, which is equivalent to 10–16 Ca^{2+} and 6.7–10 Mg^{2+} per nucleosome (200 bp). In addition, after scanning across chromosomes, we also determined a 3:1 concentration ratio of Ca^{2+} to Mg^{2+} on the chromatid axis, supporting that Ca^{2+} is enriched at the AT-rich axes.

Ca^{2+} and Mg^{2+} are essential for the integrity of chromosome structure

Previous investigations have demonstrated that incubation of cells with chelators results in partially decondensed mitotic chromosomes (Zelenin et al., 1982; Herzog and Soyer, 1983; Earnshaw and Laemmli, 1983; Staron, 1985). These studies also showed rescue of the condensed chromosome state after addition of Ca^{2+} or Mg^{2+}. To quantitate the chromosomal loss of cations due to chelators and identify cation–protein interactions, IM cells were released from a G_2/M phase block and then depleted of divalent cations using the chelators BAPTA-AM/BAPTA or EGTA as they entered mitosis. Cation-depleted chromosomes were then isolated and analyzed for Ca^{2+} and Mg^{2+} by imaging SIMS. The ion-induced secondary ion (ISI) topographical maps, and the images obtained using fluorescent DAPI (Figs. 6 and 7) and YOYO-1 staining, exhibited highly swollen partially decondensed chromosome structures, in contrast to the compacted control chromosomes. Using for example 5 mM EGTA, a 5-fold and 10-fold reduction of Mg^{2+} and Ca^{2+} occurred at the chromosomes, respectively (Figs. 6, E and F, and 7 D). We also observed sister chromatid disjunction (except at the centromeres) (Figs. 6 I and 7 A, arrows).

We further examined the Ca^{2+} and Mg^{2+} depleted chromosomes for cation–protein interactions by immunofluorescence (IF) and immunoblotting using specific antibodies against histone H1 and the nonhistone scaffold proteins Topo II, ScII, and hCAP-C. A 10-fold reduction of antibody staining for Topo II and ScII proteins was observed after Ca^{2+}/Mg^{2+} depletion (Fig. 7, A–D), which was confirmed using SDS gel electrophoresis and immunoblotting (Fig. 7, B and C). In contrast, the condensation protein hCAP-C, the linker histone H1 and the core histones, remained bound on Ca^{2+}- and Mg^{2+}-depleted chromosomes using IF and immunoblotting (Figs. 6, H and J, and 7, B and C). In particular, IF staining for histone H1 on isolated Ca^{2+}- and Mg^{2+}-depleted chromosomes showed similar signal intensities to the control chromosomes, but the chromatin was partially decondensed (Fig. 6, H and J).

Ca^{2+} directly binds and inactivates the enzymatic activity of chromosomal Topo II

It is well documented that Topo II localizes at the mitotic chromosome axes (Earnshaw et al., 1985; Saitoh and Laemmli, 1994). From our SIMS analyses, we derived a ratio of 3:1 Ca^{2+}/Mg^{2+} on the chromosomal axis (Figs. 4 and 5). Therefore, we determined the Topo II enzymatic activity in vitro in the presence of different cation concentration ratios. This assay determines the Topo II relaxation

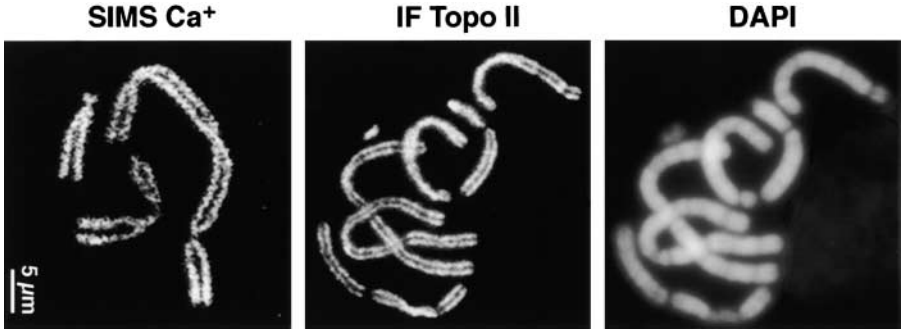

Figure 5. **Colocalization of the Topo II scaffolding protein (IF Topo II) and the Ca^{2+} distribution (SIMS Ca^{2+}) on IM metaphase chromosomes by IF using a Topo II antibody.** The Ca^{2+} SIMS map also shows a fine spiraling structure of the chromatid axes.

activity of negatively supercoiled plasmid DNA or catenated kinetoplast DNA in the presence of Mg^{2+}, which is essential for catalytic activity (Osheroff and Zechiedrich, 1987). Our results showed that Topo II activity was inhibited 57–90% when the molar ratio of Ca^{2+}/Mg^{2+} was in the range 1:1–3:1, respectively (Fig. 8 A). This supports the notion that Topo II may be enzymatically inactive at the metaphase chromosome axes.

To directly detect Ca^{2+} binding on chromosomal proteins, we applied the fluorescent filter binding assay using the Ca^{2+} marker quin-2, which has a Ca^{2+} binding constant of 1.3×10^7 (Tatsumi et al., 1997). Although fluorescent Ca^{2+} markers, like quin-2, have difficulties detecting Ca^{2+} inside of cells (McCormack and Cobbold, 1991), these markers are more sensitive than ^{45}Ca for detecting Ca^{2+}-binding proteins directly on polyvinyldifluoride (PVDF) membranes after SDS gel electrophoresis (Tatsumi et al., 1997). In addition to known Ca^{2+}-binding control proteins, like calmodulin and albumin (Tatsumi et al., 1997), we also observed direct Ca^{2+} binding with both purified human Topo II and chromosomal IM Topo II (Fig. 8 B). In contrast, no Ca^{2+} binding was detected with other chromosomal binding proteins, including hCAP-C, ScII, and histones.

Discussion

This study has directly analyzed the cation composition of cryopreserved mammalian interphase and mitotic cells, as well as fractionated untreated and cation-depleted chromosomes at a resolution of 50 nm using SIMS. Quantitative direct SIMS imaging of cryopreserved cells demonstrated that Na^+ and K^+ were associated with chromatin throughout the cell cycle, whereas in contrast Ca^{2+} and Mg^{2+} exhibited a localization change during interphase (mainly cytoplasm) and mitosis (chromatin). Our study provides the first high resolution images of cations inside interphase and mitotic cells without using fluorescent dyes and confirms the SIMS analysis of Chandra et al. (1984) using rat interphase cells at a resolution of ~500 nm. The direct association of Ca^{2+}, Mg^{2+}, Na^+, and K^+ with cryopreserved mitotic chromatin and fractionated mitotic chromosomes finally confirms earlier experiments of cation binding to DNA and chromatin in vitro. Using SIMS and Ca^{2+} calibration standards in agarose, we quantified 7–9 mM in interphase and 4–8 mM in mitotic cells, and 12–24 mM peak intensities on mitotic chromatin (Table I). Comparable Ca^{2+} concentrations were detected in different cells, but they were detected using X-ray microanalysis and different ion calibration matrices. For example, with similar cell prepara-

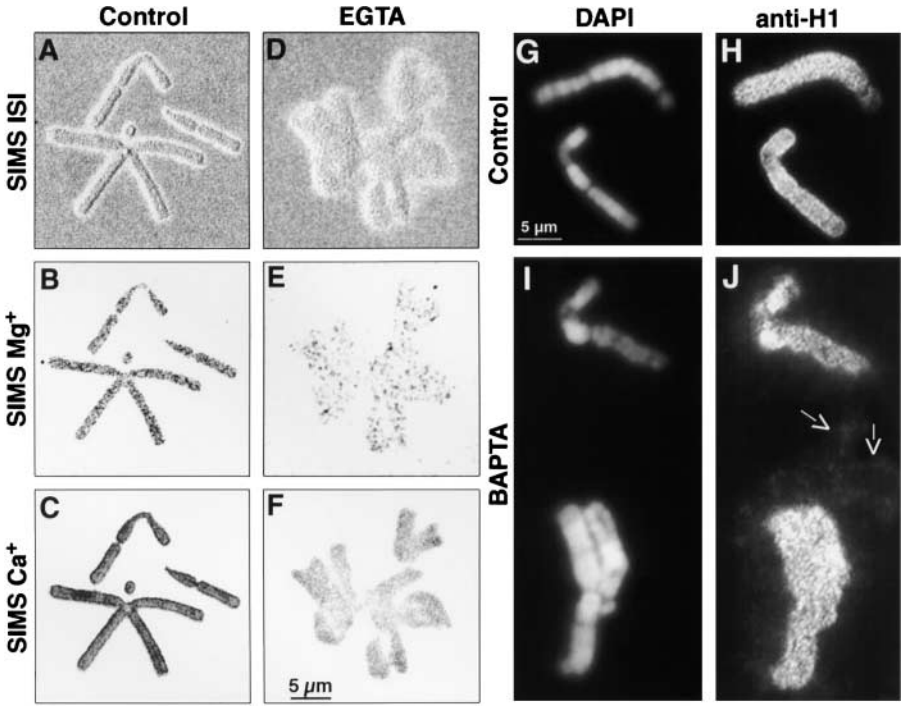

Figure 6. **Depletion of divalent cations by the chelator EGTA in G_2/M-synchronized IM cells affects the structure of chromosomes.** A–C depicts the ISI topography and SIMS Mg^{2+} and Ca^{2+} distribution maps for a control set of IM chromosomes that are compared with IM chromosomes from EGTA-cultured cells (D–F). The latter exhibit partially decondensed chromosomes, and a 5- and 10-fold reduction occurred relative to the control for Mg^{2+} and Ca^{2+}, respectively. IM control (G and H) and BAPTA-treated chromosomes (I and J) were fractionated and fixed with 4% *p*-formaldehyde and analyzed for histone H1 protein using IF. Note the partial chromosome decondensation after Ca^{2+} depletion with BAPTA-AM/BAPTA manifested with DAPI and anti-H1 antibody staining. The arrows show decondensed chromatin associated with H1.

Table I. **Ca^{2+} and Mg^{2+} concentrations in interphase and mitotic cells**

	Ca			Mg		
	Interphase	**Mitosis**	**I:M**	**Interphase**	**Mitosis**	**I:M**
Nuclei/chr.	4–6 (5.0)	12–24 (18.0)	0.28:1	2–4 (3.0)	5–17 (11.0)	0.27:1
Cytosol	5–8 (6.5)	4–6 (5.0)	1.3:1	2–3 (2.5)	2–3 (2.5)	1:1
Chromosome	ND	20–32 (26.0)	ND	ND	12–22 (17.0)	ND
Entire cell	7–9 (8.0)	4–8 (6.0)	1.3:1	1–3 (2.0)	1–3 (2.0)	1:1

Range and midrange (in parentheses) of cation concentration values in mM from different cryopreserved cells (n = 20, samples from Figs. 1 and 2 and unpublished data). The first line refers to measurements of peak intensity levels observed for nuclei and chromatin. The second line indicates average values for the cytosol. The third line gives values averaged over entire fractionated chromosomes (samples from Figs. 3–6). The fourth line represents the total Ca^{2+} and Mg^{2+} concentrations averaged over the entire cell. chr., chromatin; I:M, interphase/mitosis ratio.

tion techniques, a cellular Ca^{2+} concentration of ~8.8–10.2 mM was detected in rabbit cells (Wroblewski et al., 1983) and ~4.7–7.3 mM in T cells (Kendall et al., 1985), but using gelatin as a calibration matrix. A Ca^{2+} concentration of ~2.4–3.4 mM was found in mouse interphase cells, but a concentration ~9.5–11.0 mM was found at metaphase chromatin using X-ray microanalysis and BSA as a calibration matrix (Cameron et al., 1979). The increase of Ca^{2+} localized to mitotic chromatin compared with interphase nuclei was approximately eightfold in Cameron et al. (1979) and 3.6-fold using SIMS (Table I). However, we determined that the total cellular Ca^{2+} and Mg^{2+} concentrations between interphase and mitosis changed only minimally. We propose that during the cell cycle an intracellular redistribution of Ca^{2+} and Mg^{2+} occurs, but with no major cellular influx/efflux of these cations.

Our main research interests have focused on cation–DNA and cation–protein interactions in terms of their roles in higher order structure. Therefore, the chromatin association of Na^{+} and K^{+} supports important roles of these cations in both interphase and mitotic chromatin compaction, whereas Ca^{2+} and Mg^{2+} binding points to an essential function in mitotic chromatin compaction. Consequently, the depletion of Ca^{2+} and Mg^{2+} mitotic chromosomes, which resulted in partly decondensed structures, a process which is reversible (Zelenin et al., 1982; Earnshaw and Laemmli, 1983; Staron, 1985), points to key roles for Ca^{2+} and Mg^{2+} in specific cation–chromatin binding and in the dynamics of chromatin condensation and decondensation. DNA condensation is a multimolecular, highly cooperative and delicately balanced process, which occurs in a rapid time span during each cell

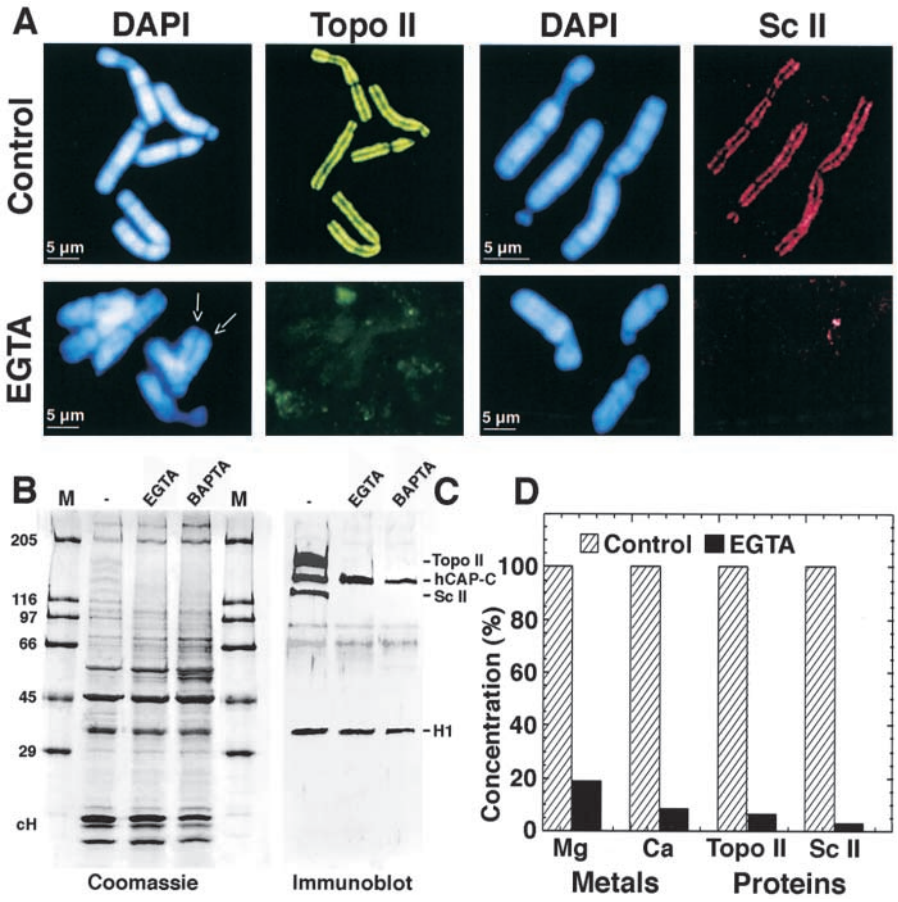

Figure 7. **IM control and EGTA-treated chromosomes, fractionated and fixed in 4% *p*-formaldehyde, were compared for chromatin proteins using IF.** (A) Topo II and ScII colocalized to the chromatid axis in the control chromosomes, whereas a loss of both proteins was detected after EGTA treatment. Similar results were obtained after BAPTA-AM/BAPTA treatment (unpublished data). The arrows in the DAPI panel indicate progressive sister chromatid disjunction, which occurred in >60% of EGTA-treated chromosomes, and in >90% of BAPTA-treated chromosomes. (B and C) The protein profile of equal amounts (10^5) of IM control (−) and IM chromosomes after EGTA or BAPTA-AM/BAPTA treatment were analyzed on an 8–15% SDS gel by electrophoresis (M, marker proteins in kD) (B) and by immunoblotting (C) using antibodies against Topo II, hCAP-C, ScII, and histone H1. Note the similar intensity of core histones (cH) in all three chromosome preparations (B), and a depletion of Topo II and ScII, but not for hCAP-C and H1 (C). (D) Histogram summarizing quantitatively the chromosomal cations and protein depletions resulting from EGTA treatment. The percentages plotted were derived from the relative signal intensities for Mg^{2+} and Ca^{2+} as well as for Topo II and ScII in a comparison between control and EGTA-treated chromosomes.

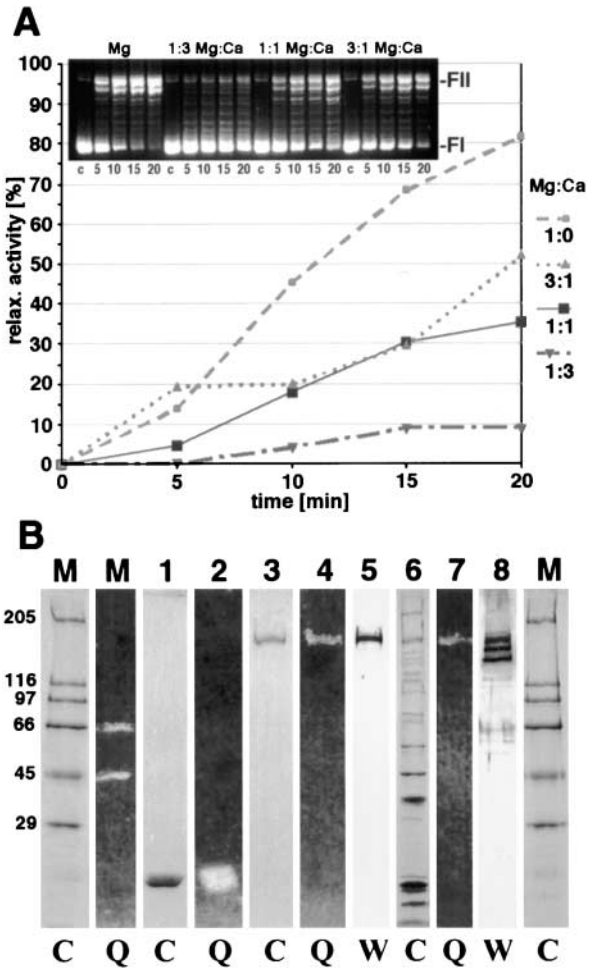

Figure 8. **Topo II directly binds Ca^{2+}, which inhibits the catalytic activity.** (A) Topo II relaxation activity inhibited by Ca^{2+} in vitro. Supercoiled plasmid DNA and 1 U of purified human Topo II in the presence of different Mg^{2+}/Ca^{2+} ratios were incubated for 5–20 min at 30°C. The inlay shows a 1.5% agarose gel of the relaxation experiments with supercoiled (FI) and relaxed (FII) forms after incubation with Topo II. Note the 1:3 Mg^{2+}/Ca^{2+} ratio detected at metaphase chromosomes using SIMS reduced the Topo II relaxation activity >90%. (B) Direct detection of Ca^{2+}-binding proteins: SDS gradient gels were stained with Coomassie blue (C) (M, marker, 1,3, and 6) or transferred to PVDF membranes, incubated with 1 mM $CaCl_2$ and then with 1 mM quin-2 (Q) and photographed after illumination with UV light (M, 2,4, and 7) or incubated with Topo II antibodies (5) or with Topo II, hCAP-C and ScII-specific antibodies (8) in Western analysis (W). Protein marker (M) (Sigma-Aldrich) represents 0.35 μg of each protein: rabbit myosin (205 kD), *E. coli* galactosidase (116 kD), rabbit phosphorylase b (97.4 kD), bovine albumin (66 kD), egg albumin (45 kD), and bovine carbonic anhydrase (29 kD). As a positive control, we used 0.75-μg bovine calmodulin (Sigma-Aldrich) (17 kD) (1 and 2). (Lanes 3,4, and 5) 5 U of purified human Topo II (TopoGen) are shown. Lanes 6, 7, and 8 represent purified fractionated IM chromosomes.

cycle. In the presence of cations, DNA condensation is determined by charge neutralization and not by binding to DNA per se as determined by calculations of electrostatic forces (for review see Bloomfield, 1998). The binding of cations specifically to the DNA phosphates results in decreasing the overall electrostatic Coulomb repulsion between free phosphates and adjacent DNA structures. For example, the DNA neutralization fraction of core histones was calculated at 57% by circular dichroism of nucleosome cores (Morgan et al., 1987, and references therein). Therefore, the remaining 43% of the DNA net negative charge must be neutralized by histone H1, the nonhistone proteins, polyamines, like spermine^{4+}, spermidine^{3+}, and putrescine^{2+}, and especially Ca^{2+}, Mg^{2+}, Na^+, and K^+. As shown for DNA oligomer crystals (Minasov et al., 1999), the DNA charge neutralization of Ca^{2+}, Mg^{2+}, Na^+, and K^+ together resulted in a greater DNA radius reduction. The effect of Ca^{2+} and Mg^{2+} on DNA compaction and overwinding has been shown with supercoiled DNA (Adrian et al., 1990) as well as with helical DNA (Xu and Bremer, 1997). The potential of cation binding for chromosome condensation and maintenance can be seen with histone-free dinoflagellate chromosomes, which are exclusively compacted and stabilized by Ca^{2+} and Mg^{2+}, at two different binding sites (Herzog and Soyer, 1983). For naked DNA, the maximal binding and compaction for Ca^{2+} and Mg^{2+} was found to be 0.63 cations/bp (or one every 3.17 nucleotides) (Koltover et al., 2000). From our total Ca^{2+} and Mg^{2+} chromosome concentration values, we determined that one Ca^{2+} binds to every 12.5–20 nucleotides (1–2 helical turns) and one Mg^{2+} to every 20–33 nucleotides (2–3 helical turns). The discrepancy between naked DNA and chromatin can be explained due to the occupation of cation binding sites with Na^+, K^+, and chromatin binding proteins. In addition, even after incubating IM cells with 10 μM of the Ca^{2+} specific ionophore A23187 for 6 h, we detected no further increase in concentration levels of Ca^{2+} or other cations tested for binding on mitotic chromosomes (unpublished data). This finding supports the notion that metaphase chromosomes have no additional binding sites for Ca^{2+} or other cations. Therefore, we conclude that the detected Ca^{2+}, Mg^{2+}, Na^+, and K^+ cations together with polyamines, histones, and nonhistone proteins result in charge neutral mitotic chromosomes and represent the highest compacted state. During cation neutralization, this process may lead to modifications in local DNA structures, like bending toward the neutralized region, and thus facilitate nucleosome folding. Subsequently, the charge neutralization of chromosomes may be necessary to facilitate free chromosomal movement throughout mitosis.

In addition to the overall chromosome binding of Ca^{2+}, Mg^{2+}, Na^+, and K^+, we also detected that Ca^{2+} specifically binds to the chromosome axis, the location of the scaffold proteins and the highly AT-rich SARs, in a 3:1 Ca^{2+}/Mg^{2+} ratio. Different DNA binding properties of Ca^{2+} and Mg^{2+} have been shown in DNA oligomer crystals where both divalent cations bound to the DNA phosphate groups over oxygen atoms; but in contrast to Mg^{2+}, Ca^{2+} was specifically found in the minor groove of AT-rich DNA (Minasov et al., 1999). Recent NMR studies of DNA oligomeres in the presence of K^+ demonstrated a stabilization of quadruplex DNA structures as implicated at the telomeres and centromeres (Marathias and Bolton, 2000). The K^+ nucleolar enrichment we observed may reflect the centromeric regions mapping adjacent to the nucleolar organizing regions. Lewis and Laemmli (1982) proposed that Cu^{2+} or Ca^{2+} is needed for stabilization of chromosome scaffolding proteins, including Topo II (ScI) and ScII. It has previously been shown that

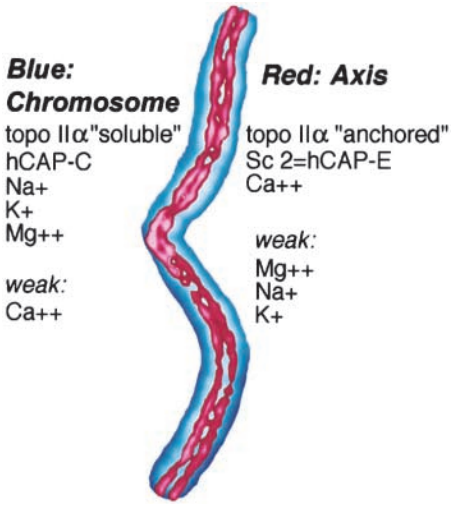

Figure 9. **Mitotic chromosome model summarizing the SIMS and IF results.** Shown are the strong and weaker signals for the different chromosome substructures. We hypothesize two different functional Topo II subspecies at mitosis, which differ in phosphorylation and Ca^{2+} association (unpublished material). Hyperphosphorylated and Ca^{2+}-associated Topo II is a DNA structural protein primarily bound to the chromosome axis (anchored or nonsalt extractable; Earnshaw et al., 1985). The hypophosphorylated and non–Ca^{2+}-associated Topo II is catalytically active and bound to the nonaxis part of chromosomes (soluble or salt extractable; Hirano and Mitchison, 1993).

10% of the total nuclear Ca^{2+} is bound to the nonhistone–scaffold protein fraction (Schibeci and Martonosi, 1980). Our direct binding experiments of Ca^{2+} with Topo II supports that Topo II is the main Ca^{2+}-binding protein in the scaffold fraction (Fig. 8 B). Since we demonstrated that Ca^{2+} and not Cu^{2+} is enriched on the chromosomal axis using SIMS, we propose that Ca^{2+} is the most likely candidate for stabilization of the chromosomal scaffolding proteins, particularly Topo II. The finding of Lewis and Laemmli (1982) concerning the role of Cu^{2+} can be explained in that, in contrast to Ca^{2+}, Cu^{2+} can bind multiple oxygen atoms of proteins with the result of oxidizing the peptide backbone and being reduced to Cu^{+} (Legler et al., 1985). The fact that Ca^{2+} also widened the minor groove, whereas Mg^{2+} contracted it (Minasov et al., 1999), may also have important implications for the structure and function of SARs at the chromosome axes as well as for axis-binding proteins like Topo II and ScII.

Topo II and ScII proteins comprise ~40% of the overall proteins in the chromosome scaffold (Earnshaw and Laemmli, 1983), and are involved in chromosome structure maintenance at the chromosome axes (Boy de la Tour and Laemmli, 1988; Saitoh et al., 1994). Andreassen et al. (1997) colocalized Topo II and ScII only after prophase on the axes, supporting that the mitotic ScII may be present in two complexes, with the condensins and with Topo II. We showed that Topo II directly binds Ca^{2+} without binding DNA, whereas chromosomal ScII did not (Fig. 8 B), although Ca^{2+} chelation experiments depleted Topo II and ScII from mitotic chromosomes (Fig. 7). This result could be explained that Topo II binds to both Ca^{2+} and ScII and after chelation of Ca^{2+} both proteins are depleted due to possible strong protein–protein binding (Lewis and Laemmli, 1982; Ma et al., 1993). We observed that over 80–90% chelation of chromosome bound Ca^{2+} and Mg^{2+} resulted in partially decondensed chromosomes and, more importantly, in a 90–95% loss of Topo II and ScII, but in no loss of hCAP-C and histones. These partially decondensed structures are most likely due to both the loss of compaction and neutralization by Ca^{2+} and Mg^{2+}, as well as by the simultaneous depletion of Ca^{2+}/Mg^{2+}-bound Topo II. A complete chromosome collapse was not detected because of the remaining Na^{+} and K^{+}, histones, and other nonhistone proteins, like hCAP-C as well as DNA–DNA interactions.

Finally, we found that the 3:1 chromosome axis ratio of Ca^{2+}/Mg^{2+} fully inhibited Topo II catalytic activity in vitro (Fig. 8 A). In Ca^{2+} and Mg^{2+} competition studies by us and Osheroff and Zechiedrich (1987), results showed that an interaction between Ca^{2+} and Topo II led to inactivation of the catalytic activity by trapping Topo II onto DNA in a stabilized cleavage complex. It is reasonable that the recent findings of catalytically inactive Topo II on chromosomes at metaphase and especially anaphase (Shamu and Murray, 1992; Meyer et al., 1997; Bojanowski et al., 1998) may be explained by Ca^{2+} binding, and that the actual mechanism involving Ca^{2+}-induced Topo II enzymatic inactivation could be due to the larger ionic radii of Ca^{2+} (0.99A) as compared with Mg^{2+} (0.66 A), thus altering the tertiary structure of Topo II and converting it to a solely structural DNA binding protein. If Topo II has two (or more) different binding sites for Ca^{2+} and Mg^{2+} like DNase A (Poulos and Price, 1972) or only one site is still unresolved. Interestingly, in the presence of Ca^{2+}, DNase A had different DNA cleavage specificity and changes of the protein structure protecting the enzyme against proteolysis (Poulos and Price, 1972). It will be important to determine if the enzymatic activity of Topo II is inhibited after binding of Ca^{2+} due to the changing of protein structure.

The G2 checkpoint of mammalian cells requires Topo II–dependent decatenation of DNA duplexes before entry in mitosis (Downes et al., 1994). Topo II specific drugs, like VP16 given in G1 or S phase inhibit Topo II, resulting in undecatenated DNA and G2 arrest (Tobey et al., 1990). Ca^{2+} binds Topo II and DNA in a covalent complex, but leaves Topo II kinetically active (Osheroff and Zechiedrich, 1987). In contrast to VP16, a depletion of Ca^{2+} at the chromatin due to the redistribution during the cell cycle could result in active Topo II, religating DNA cleavages, and thus, explain the lack of DNA breaks during/after mitosis. After prophase, the cells are insensitive to Topo II inhibitors (Rowley and Kort, 1989), presumably because chromosomal Topo II is complexed with Ca^{2+} and DNA as stable cleavage complexes.

In conclusion, this investigation identifies the cations Ca^{2+}, Mg^{2+}, Na^{+}, and K^{+} as essential participants in the maintenance of higher order structure in mammalian chromosomes particularly at mitosis due to their functions in (a) DNA electrostatic neutralization and chromosome condensation, (b) a direct interaction of Ca^{2+} with Topo II, and (c) regulation of Topo II as a structural chromosomal binding protein through cation–protein interactions with Ca^{2+} at

the chromosomal axis. The distribution of these chromatin-binding cations and the scaffold proteins are represented in our chromosome model (Fig. 9). Thus, the cations Ca^{2+}, Mg^{2+}, Na^{+}, and K^{+} in addition to polyamines, histones, and nonhistone proteins are pivotal to complete and maintain "maximal chromosome condensation" during mitosis.

Materials and methods

Scanning ion microprobe

In the University of Chicago scanning ion microprobe (Chabala et al., 1995), a 30-pA beam of gallium ions extracted from a liquid metal ion source, typically accelerated to 45 keV and focused to a spot ~50 nm in diameter, is rastered over a specimen to erode the outer surface layers. The sputtered ionized atoms or molecular clusters are discriminated on the basis of their mass/charge ratio with a high performance magnetic sector mass spectrometer (Finnigan MAT 90). Both positive and negative ion species can be mass analyzed. By recording the secondary ion signal counts, detected by an active film electron multiplier (ETP AF820), as a function of the position of the scanning beam, two-dimensional compositional distribution (SIMS) maps are obtained. The sputter erosion depth during the acquisition of one analytical image (map), inverse function of the magnification, can be controlled over a wide range from a few atomic monolayers to tens of nanometers. A detector overlooking the sample collects secondary ions yielding topographic (ISI) images similar to those generated by a scanning electron microscope. The detection sensitivity in analytical images can reach the ppm range, due to the high transmission efficiency (~20%) of the SIMS system. The digital images, containing 512 × 512 picture elements from single square raster scans are analyzed with a KONTRON IMCO image processing system.

Cell lines and culture

Male IM deer primary fibroblast cells (American Type Culture Collection) and the BV173 human leukemia T/B-progenitor cell line (gift from Dr. J.D. Rowley, University of Chicago, Chicago, IL) were grown in log phase from previously seeded cell cultures at 0.07×10^6 cells/ml in F10 media (Life Technologies), 10% FCS, or 0.5×10^6 cells/ml in RPMI (Life Technologies) with 10% FCS, respectively.

Cryopreservation and fracturing of cells

The cryopreservation was performed according to Chandra et al. (1986) with modifications. IM cells were grown on 99.99% pure silicon substrate discs, or fractionated mitotic cells were layered onto silicon discs and immediately dipped into a liquid N_2 plus 1,1,1-trichloroethane slush bath (−150°C) at a speed of 2 m/s to a depth of 5 cm for 10 s. Cryofracturing of cells was obtained by splitting open a sandwich of two discs. The frozen discs were then transferred under N_2/1,1,1-trichloroethane into a –65°C vacuum chamber for 16 h at a pressure of 0.5 millitorr and then brought to room temperature in 2 h under vacuum.

Cell synchronization

IM and BV173 cells were synchronized at the G1/S phase border using aphidicolin (20 μM) for 16 h. The block was then released for 3 h, and 0.3μM nocodazole was added for an additional 18 h. Mitotic cells were collected in the supernatant fraction, and DAPI staining showed >98% pro- or metaphase cells with only 1–2% interphase cells. For experiments involving chelators, we first synchronized IM cells to the G1/S border and then added 0.2 μM nocodazole for 18 h. Using this approach, >80% of the total cells were synchronized to the G2/M border, as determined by optical microscopy and DAPI staining. After releasing the G2/M block, either EGTA (5 mM) or EDTA (5 mM) or BAPTA (0.3 mM) and BAPTA-AM (50 μM) was added for 6 h, and mitotic chromosomes were harvested using the chromosome isolation methods described below for comparison.

Chromosome harvests

Two chromosome harvesting procedures were used for SIMS and IF analysis. In one method, chromosomes were extracted from mitotic cells and then fixed in methanol: acetic acid (3:1) according to Ohnuki (1968). This extraction method could lead to artifacts by contaminating chromosomes with cytosolic cations. Therefore, individual IM and BV173 metaphase chromosomes were also fractionated from cells that preserve the morphological integrity of chromosomes as shown by Saitoh and Laemmli (1994). Briefly, after cells were synchronized at mitosis, chromosomes were isolated in Ca^{2+}- and Mg^{2+}-free buffers using a glycerol step-gradient and then fixated with 4% *p*-formaldehyde. For SIMS analysis, chromosome samples were mounted onto alumina ceramic coverslips, which are devoid of innate K^{+}, Na^{+}, Ca^{2+}, and Mg^{2+} ions, previously lightly Au coated to ensure substrate conductivity, and then air-dried. The samples were further coated with a thin sputter-deposited layer of gold to prevent electrical charging.

Immunofluorescence

IM and BV173 fractionated chromosomes were fixed with 4% *p*-formaldehyde and incubated with anti–Topo II monoclonal (Boehringer), anti-ScII polyclonal (Saitoh et al., 1994), anti-H1 monoclonal (Biodesign), and anti–hCAP-C polyclonal (Schmiesing et al., 1998) antibodies, diluted 1:200, 1:50, 1:30, and 1:100, respectively, with 3% BSA in PBS. Rhodamine-conjugated anti–mouse or anti–rabbit secondary antibodies (Boehringer) were used in a dilution of 1:150. The chromosomes were analyzed with a ZEISS Axioplan microscope combined with a digital CCD camera.

Quantitation of Ca^{2+} and Mg^{2+} on chromosomes

We established a Ca^{2+} and Mg^{2+} reference for SIMS using different concentrations of Ca^{2+} and Mg^{2+} mixed with high purity agarose (Seakem Gold, FMC) as a matrix. We also established Cu^{2+} references for SIMS. Agarose was chosen as a carrier because of the comparable chemical structure to DNA (parallel double helix with left-handed symmetry, tightly bound water, and similar relative density to DNA, which we determined to be equal 1.869 kg/l). Drying of agarose, necessary for SIMS analysis, has only minimal impact on structure (Arndt and Stevens, 1994). The standards were solubilized in bidistilled water, deposited on Au-coated glass coverslips, vacuum dried, Au coated, and mass analyzed for Ca^{2+} and Mg^{2+} using SIMS. Control agarose samples were also SIMS analyzed, indicating negligible Ca^{2+} and Mg^{2+} background. SIMS sensitivity was greater than 10^{-8} M for $^{40}Ca^{2+}$ and greater than 10^{-7} M for $^{24}Mg^{2+}$ and $^{63}Cu^{2+}$. Calibration plots of SIMS signal intensity (cts/pxl) corresponding to different cation concentrations are shown in Fig. 4, G and H. The number of metal atoms/nucleotide was obtained by multiplying the measured local metal atomic concentration (in ppm) by the average number of atoms/nucleotide (taken as 36) divided by 10^6.

Fluorescent filter-binding assay for the detection of Ca^{2+}-binding proteins

The assay was performed according to Tatsumi et al. (1997), except using $MgCl_2$ in the washing buffer. Protein marker and Calmodulin (Sigma-Aldrich), purified human Topo II (TopoGen), and fractionated IM chromosomes were electrophoresed on a 7.5–15% SDS gradient gel and transferred onto PVDF membrane (Bio-Rad Laboratories). After incubating the membrane with 1 mM $CaCl_2$ and then with quin-2 (Sigma-Aldrich) for 1 h, the fluorescent proteins (Ca^{2+}-binding proteins) were visualized by illumination with UV light at 365 nm, digitally photographed, and analyzed with the Kodak 1D Imaging system.

Topo II relaxation reaction

0.2 μg of supercoiled plasmid pSP72 (Promega) DNA was incubated at 30°C for 5–20 min in the presence of 1 U of purified human Topo II (TopoGen) and Ca^{2+} and Mg^{2+} in different ratios in a Topo II relaxation buffer (Osheroff and Zechiedrich, 1987). The reaction was stopped with 1% SDS and 15 mM EDTA, and the DNA phenol/chloroform was extracted, ethanol precipitated, and analyzed on a 1.5% agarose gel. The Topo II relaxation activity was quantified using the ImageQuant analysis program (Molecular Dynamics).

We wish to thank Dr. J.D. Rowley for her support and L. Gavrilov for expert technical assistance. We are grateful to Dr. W.C. Earnshaw for providing the ScII antibodies and to Dr. K. Yokomori for the hCAP-C antibodies.

At the Enrico Fermi Institute (Chicago, IL), this work was supported by a grant from the Pritzker Foundation.

References

Adachi, Y., M. Luke, and U.K. Laemmli. 1991. Chromosome assembly in vitro: topoisomerase II is required for condensation. *Cell.* 64:137–148.

Adrian, M., B. ten Heggeler-Bordier, W. Wahli, A.Z. Stasiak, A. Stasiak, and J. Dubochet. 1990. Direct visualization of supercoiled DNA molecules in solution. *EMBO J.* 9:4551–4554.

Andreassen, P.R., F.B. Lacroix, and R.L. Margolis. 1997. Chromosomes with two intact axial cores are induced by G2 checkpoint override: Evidence that DNA decatenation is not required to template the chromosome structure. *J. Cell Biol.* 136:29–43.

Arndt, E.R., and E.S. Stevens. 1994. A conformational study of agarose by Vacuum UV CD. *Biopolymers.* 34:1527–1534.

Atkinson, M.J., C. Cade, and A.D. Perris. 1983. Sodium and ouabain induce proliferation of rat thymic lymphocytes via calcium- and magnesium-dependent reactions. *Cell Calcium.* 4:1–12.

Benninghoven, A. 1987. Secondary Ion Mass Spectrometry. A. Benninghoven, F.G. Rüdenauer, and H.W. Werner, editors. John Wiley & Sons, New York. 1227 pp.

Bloomfield, V.A. 1998. DNA condensation by multivalent cations. *Biopolymers.* 44:269–282.

Bojanowski, K., A.J. Maniotis, S. Plisov, A.K. Larsen, and D.E. Ingber. 1998. DNA topoisomerase II can drive changes in higher order chromosome architecture without enzymatically modifying DNA. *J. Cell. Biochem.* 69:127–142.

Boy de la Tour, E., and U.K. Laemmli. 1988. The metaphase scaffold is helically folded: sister chromatids have predominantly opposite helical handedness. *Cell.* 55:937–944.

Boynton, A.L., W.L. McKeehan, and J.F. Whitfield. 1982. Ions, cell proliferation, and cancer. Academic Press, New York. 551 pp.

Cameron, I.L., N.K. Smith, and T.B. Pool. 1979. Element concentration changes in mitotically active and postmitotic enterocytes. An x-ray microanalysis study. *J. Cell Biol.* 80:444–450.

Chabala, J.M., K.K. Soni, J. Li, K.L. Gavrilov, and R. Levi-Setti. 1995. High resolution chemical imaging with scanning ion probe SIMS. *Int. J. Mass Spectrom., and Ion Processes.* 143:191–212.

Chandra, S., W.C. Harris, and G.H. Morrison. 1984. Distribution of calcium during interphase and mitosis as observed by ion microscopy. *J. Histochem. Cytochem.* 32:1224–1230.

Chandra, S., G.H. Morrison, and C.C. Wolcott. 1986. Cell culture freeze-fracture for ion microscopy. *J. Microscopy.* 144:15–37.

Chiu, T.K., and R.E. Dickerson. 2000. 1 A crystal structures of B-DNA reveal sequence-specific binding and groove-specific bending of DNA by magnesium and calcium. *J. Mol. Biol.* 301:915–945.

Downes, C.S., D.J. Clarke, A.M. Mullinger, J.F. Gimenez-Abian, A.M. Creighton, and R.T. Johnson. 1994. A topoisomerase II-dependent G2 cycle checkpoint in mammalian cells. *Nature.* 372:467–470.

Earnshaw, W.C., and U.K. Laemmli. 1983. Architecture of metaphase chromosomes and chromosome scaffolds. *J. Cell Biol.* 96:84–93.

Earnshaw, W.C., B. Halligan, C.A. Cooke, M.M. Heck, and L.F. Liu. 1985. Topoisomerase II is a structural component of mitotic chromosome scaffolds. *J. Cell Biol.* 100:1706–1715.

Echlin, P. 1984. Analysis of organic and biological surfaces. P.J. Elving, and J.D. Winefordner, editors. John Wiley & Sons, Chemical analysis. *Vol.* 71:529–557.

Felsenfeld, G., and J.D. McGhee. 1986. Structure of the 30 nm chromatin fiber. *Cell.* 44:375–377.

Filipski, J., J. Leblanc, T. Youdale, M. Sikorska, and P.R. Walker. 1990. Periodicity of DNA folding in higher order chromatin structures. *EMBO J.* 9:1319–1327.

Groigno, L., and M. Whitaker. 1998. An anaphase calcium signal controls chromosome disjunction in early sea urchin embryos. *Cell.* 92:193–204.

Hammarsten, E. 1923. Zur Kenntnis der biologischen Bedeutung der Nukleinsaeureverbindungen. *Biochem. Z.* 144:383–466.

Hepler, P.K. 1994. The role of calcium in cell division. *Cell Calcium.* 16:322–330.

Herzog, M., and M.O. Soyer. 1983. The native structure of dinoflagellate chromosomes and their stabilization by Ca^{2+} and Mg^{2+} cations. *Eur. J. Cell Biol.* 30: 33–41.

Hirano, T., and T.J. Mitchison. 1993. Topoisomerase II does not play a scaffolding role in the organization of mitotic chromosomes assembled in Xenopus egg extracts. *J. Cell Biol.* 120:601–612.

Hirano, T. 1999. SMC-mediated chromosome mechanics: a conserved scheme from bacteria to vertebrates? *Genes Dev.* 13:11–19.

Horoyan, M., M. Soler, A.M. Benoliel, M. Fraterno, M. Passerel, H. Subra, J.M. Martin, P. Bongrand, and C. Foa. 1992. Localization of calcium changes in stimulated rat mast cells. *J. Histochem. Cytochem.* 40:51–63.

Kearns, L.P., and D.C. Sigee. 1980. The occurrence of period IV elements in dinoflagellate chromatin: an X-ray microanalytical study. *J. Cell Sci.* 46:113–127.

Kendall, M.D., A. Warley, and I.W. Morris. 1985. Differences inapparent elemtal composition of tissues and cells using a fully quantitative X-ray microanalysis system. *J. Micros.* 138:35–42.

Koltover, I., K. Wagner, and C.R. Safinya. 2000. DNA condensation in two dimensions. *Proc. Natl. Acad. Sci. USA.* 97:14046–14051.

Legler, G., C.M. Muller-Platz, M. Mentges-Hettkamp, G. Pflieger, and E. Julich. 1985. On the chemical basis of the Lowry protein determination. *Anal. Biochem.* 150:278–287.

Levi-Setti, R. 1988. Structural and microanalytical imaging of biological materials by scanning microscopy with heavy-ion probes. *Annu. Rev. Biophys. Chem.* 17:325–347.

Levi-Setti, R., J.M. Chabala, K. Gavrilov, R. Espinosa, and M.M. Le Beau. 1997. Imaging of BrdU-labeled human metaphase chromosomes with a high resolution scanning ion microprobe. *Micros. Res. Tech.* 36:301–312.

Lewis, C.D., and U.K. Laemmli. 1982. Higher order metaphase chromosome structure: evidence for metalloprotein interactions. *Cell.* 29:171–181.

Ma, X., N. Saitoh, and P.J. Curtis. 1993. Purification and characterization of a nuclear DNA-binding factor complex containing topoisomerase II and chromosome scaffold protein 2. *J. Biol. Chem.* 268:6182–6188.

Marathias, V.M., and P.H. Bolton. 2000. Structures of the potassium-saturates, 2:1, and intermediate, 1:1, forms of a quadruplex DNA. *Nucleic Acids Res.* 28:1969–1977.

Mathieson, A.R., and J.Y. Olayemi. 1975. The interaction of calcium and magnesium ions with deoxyribonucleic acid. *Arch. Biochem. Biophys.* 169:237–243.

McCormack, J.G., and P.H. Cobbold. 1991. Cellular Calcium. IRL Press, Oxford University Press.

Meyer, K.N., E. Kjeldsen, T. Straub, B.R. Knudsen, I.D. Hickson, A. Kikuchi, H. Kreipe, and F. Boege. 1997. Cell cycle-coupled relocation of types I and II topoisomerases and modulation of catalytic enzyme activities. *J. Cell Biol.* 136:775–788.

Minasov, G., V. Tereshko, and M. Egli. 1999. Atomic-resolution crystal structures of B-DNA reveal specific influences of divalent metal ions on conformation and packing. *J. Mol. Biol.* 291:83–99.

Morgan, A.J., T.W. Davies, and D.A. Erasmus. 1975. Changes in the concentration and distribution of elements during electron microscope preparative procedures. *Micron.* 6:11–23.

Morgan, J.E., J.W. Blankenship, and H.R. Matthews. 1987. Polyamines and acetylpolyamines increase the stability and alter the conformation of nucleosome core particles. *Biochemistry.* 26:3643–3649.

Ohnuki, Y. 1968. Structure of chromosomes. I. Morphological studies of the spiral structure of human somatic chromosomes. *Chromosoma.* 25:402–428.

Osheroff, N., and E.L. Zechiedrich. 1987. Calcium-promoted DNA cleavage by eukaryotic topoisomerase II: trapping the covalent enzyme-DNA complex in an active form. *Biochem.* 26:4303–4309.

Paulson, J.R., and U.K. Laemmli. 1977. The structure of histone-depleted metaphase chromosomes. *Cell.* 12:817–828.

Poenie, M., J. Alderton, R. Steinhardt, and R. Tsien. 1986. Calcium rises abruptly and briefly throughout the cell at the onset of anaphase. *Science.* 233:886–889.

Poulos, T.L., and P.A. Price. 1972. Some effects of calcium ions on the structure of bovine pancreatic deoxyribonuclease A. *J. Biol. Chem.* 247:2900–2904.

Rattner, J.B., and C.C. Lin. 1985. Radial loops and helical coils coexist in metaphase chromosomes. *Cell.* 42:291–296.

Rottingen, J.A., and J.G. Iversen. 2000. Ruled by waves? Intracellular and intercellular calcium signalling. *Acta Physiol. Scand.* 169:203–219.

Rowley, R., and L. Kort. 1989. Novobiocin, nalidixic acid, etoposide, and 4'-(9-acridinylamino) methanesulfon-m-anisidide effects on G2 and mitotic Chinese hamster ovary cell progression. *Cancer Res.* 49:4752–4757.

Saitoh, Y., and U.K. Laemmli. 1994. Metaphase chromosome structure: bands arise from a differential folding path of the highly AT-rich scaffold. *Cell.* 76: 609–622.

Saitoh, N., I.G. Goldberg, E.R. Wood, and W.C. Earnshaw. 1994. ScII: an abundant chromosome scaffold protein is a member of a family of putative ATPases with an unusual predicted tertiary structure. *J. Cell Biol.* 127:303–318.

Schapiro, F.B., and S. Grinstein. 2000. Determinants of the pH of the Golgi complex. *J. Biol. Chem.* 275:21025–21032.

Scheiner-Bobis, G. 1998. Ion-transporting ATPases as ion channels. *Naunyn Schmiedebergs Arch. Pharmacol.* 357:477–482.

Schibeci, A., and A. Martonosi. 1980. Ca^{2+}-binding proteins in nuclei. *Eur. J. Biochem.* 113:5–14.

Schmiesing, J.A., A.R. Ball, H.C. Gregson, J.M. Alderton, S. Zhou, and K. Yokomori. 1998. Identification of two distinct human SMC protein complexes

involved in mitotic chromosome dynamics. *Proc. Natl. Acad. Sci. USA.* 95: 12906–12911.

Shamu, C.E., and A.W. Murray. 1992. Sister chromatid separation in frog extracts requires DNA topoisomerase II activity during anaphase. *J. Cell Biol.* 117: 921–934.

Staron, K. 1985. Condensation of the chromatin gel by cations. *Bioch. Biophys. Acta.* 825:289–298.

Strick, R., and U.K. Laemmli. 1995. SARs are *cis* DNA elements of chromosome dynamics: synthesis of a SAR repressor protein. *Cell.* 83:1137–1148.

Tatsumi, R., K. Shimada, and A. Hattori. 1997. Fluorescence detection of calcium-binding proteins with quinoline Ca-indicator quin2. *Anal. Biochem.* 254: 126–131.

Tobey, R.A., N. Oishi, and H.A. Crissman. 1990. Cell cycle synchronization: reversible induction of G2 synchrony in cultured rodent and human diploid fibroblasts. *Proc. Natl. Acad. Sci. USA.* 87:5104–5108.

Warley, A., J. Stephen, A. Hockaday, and T.C. Appleton. 1983. X-ray microanalysis of HeLa S3 cells. II. Analysis of elemental levels during the cell cycle. *J. Cell Sci.* 62:339–350.

Wroblewski, J., G.M. Roomans, K. Madsen, and U. Friberg. 1983. X-ray microanalysis of cultured chondrocytes. *Scan. Electron Microsc.* 2:777–784.

Xu, Y.C., and H. Bremer. 1997. Winding of the DNA helix by divalent metal ions. *Nucleic Acids Res.* 25:4067–4071.

Zelenin, M.G., A.F. Zakharov, O.V. Zatsepina, V.Y. Polijakov, and Y.S. Chentsov. 1982. Reversible differential decondensation of unfixed Chinese hamster chromosomes induced by change in calcium ion concentration of the medium. *Chromosoma.* 84:729–736.